

# From particles to spins: Eulerian formulation of supercooled liquids and glasses

Claudio Chamon\*, Leticia F. Cugliandolo<sup>†</sup>, Gabriel Fabricius<sup>‡</sup>, José Luis Iguain<sup>§</sup>, and Eric R. Weeks<sup>¶||</sup>

\*Physics Department, Boston University, Boston, MA 02215; <sup>†</sup>Université Pierre et Marie Curie–Paris VI, Laboratoire de Physique Théorique et Hautes Énergies, Unité Mixte de Recherche 7589, 4 Place Jussieu, 75252 Paris Cedex 05, France; <sup>‡</sup>Instituto de Investigaciones Físicoquímicas Teóricas y Aplicadas, Universidad Nacional de La Plata, Consejo Nacional de Investigaciones Científicas y Técnicas de Argentina, Casilla de Correo 16, Sucursal 4 (1900) La Plata, Argentina; <sup>§</sup>Departamento de Física, FCEyN, Universidad Nacional de Mar del Plata, Deán Funes 3350, 7600 Mar del Plata, Argentina; and <sup>¶</sup>Physics Department, Emory University, Atlanta, GA 30322

Edited by Peter G. Wolynes, University of California at San Diego, La Jolla, CA, and approved July 10, 2008 (received for review March 23, 2008)

**The dynamics of supercooled liquid and glassy systems are usually studied within the Lagrangian representation, in which the positions and velocities of distinguishable interacting particles are followed. Within this representation, however, it is difficult to define measures of spatial heterogeneities in the dynamics, as particles move in and out of any one given region within long enough times. It is also nontransparent how to make connections between the structural glass and the spin glass problems within the Lagrangian formulation. We propose an Eulerian formulation of supercooled liquids and glasses that allows for a simple connection between particle and spin systems, and that permits the study of dynamical heterogeneities within a fixed frame of reference similar to the one used for spin glasses. We apply this framework to the study of the dynamics of colloidal particle suspensions for packing fractions corresponding to the supercooled and glassy regimes, which are probed via confocal microscopy.**

dynamics | structural

The phenomenology of structural and spin glasses has much in common: no static long-range order, aging relaxation, heterogeneous dynamics, and so on (for reviews, see refs. 1 and 2). Although a precise and unambiguous connection between these two problems is still lacking, the possibility that such relation exists dates back to the work by Kirkpatrick, Thirumalai, and Wolynes (3–8), who proposed a connection between structural glasses and fully connected  $p$ -spin disordered models. These mean-field spin models have a dynamic phase transition that mimics the glassy arrest at  $T_g$  and a static phase transition at a lower temperature  $T_s$  that realizes the Kauzmann entropy crisis. The spin dynamics is sluggish above and close to  $T_g$  as in supercooled liquids and the system falls out of equilibrium below  $T_g$  and shows aging as in a glass (1, 9). More recently, Tarzia and Moore (10) have paralleled the phenomenology of structural glasses to that of an Edwards–Anderson model in a uniform magnetic field. One of the main hurdles in making a direct real space connection between structural and spin glasses is that disordered spin models are defined on a lattice, whereas the particles comprising structural glasses are itinerant.

Supercooled liquids and glasses are usually described within the Lagrangian formulation, in which one tracks the position of individual particles as a function of time. Natural quantities computed within this frame of reference are the particle's mean-square displacement and self-diffusion. Heterogeneous dynamics can be probed, for example, by studying quantities such as mobility within prescribed boxes; however, such fixed regions serve this purpose just for a certain time, because particles move in and out of these boxes if one waits for long enough. In contrast, studying local dynamics in a spin glass presents no such complication, because spins remain fixed to their sites at all times, and all that changes is the spin orientation as a function of time. Therefore, if one is to construct a simple description of particle systems that could actually be used in analyzing real experimen-

tal data from the point of view of a spin glass, one must abandon the Lagrangian formulation.

We propose an Eulerian analysis of the dynamics of interacting particle systems. By working with such a fixed frame of reference and disregarding the individual particle identities, it is conceptually more natural to make a connection to lattice spin systems. Let us illustrate the idea more concretely by considering the particular case of hard spherical particles (which we explain in full detail below).\*\* We partition the whole system volume into a grid with lattice spacing  $a$  that is *smaller* than the particle radius  $R$ . In this case, a *microscopic* density  $n_i = 1, 0$  (or an associated “spin”  $s_i = \pm 1$ ) can be assigned to a given lattice point labeled by  $i$ , depending on whether a piece of the sphere overlaps or not with the box at  $i$ . One should contrast this microscopic density to a *macroscopic* one defined within boxes *larger* than the particle radius that counts the number of distinct particles within the coarse-grained volume (11).

The dynamics of the corresponding spin equivalent model is inherently constrained: a particle that moves corresponds to a correlated flip of many spins. For example, spins deep inside a domain of  $\pm 1$  spins are not allowed to be flipped if one is not to create holes inside a particle or tiny particles within the voids. (If small elastic deformations of the particles are allowed, the magnetization does not necessarily need to be conserved.) The spins susceptible to flip are those at the boundary of the particles, and there is naturally a kinetic constraint on the flipable spins that is dictated by a large number of its neighbors.

The Eulerian approach thus suggests a rather different motivation for the study of kinetically constrained systems, such as the Fredrickson–Andersen model (12, 13), in their connection to glassy dynamics. These types of models are presented as a phenomenological description where the spins correspond to certain measures of dynamic activity at large, coarse-grained length scales. Here, the physical motivation is more microscopic, and it goes in the opposite direction from looking at small length scales, lesser or comparable to the particle radii.

Given a particle radius  $R$  and the lattice scale  $a$ , one can construct an interacting spin model, with kinetic constraints that faithfully mimic the particle dynamics. Such a detailed (and evidently complicated) model would certainly be rather difficult to analyze. Its essence, nonetheless, might be captured in simpler effective lattice models. However, instead of attempting to construct and analyze such a model at this stage, we pose and

Author contributions: C.C., L.F.C., G.F., J.L.I., and E.R.W. designed research, performed research, contributed new reagents/analytic tools, analyzed data, and wrote the paper.

The authors declare no conflict of interest.

This article is a PNAS Direct Submission.

||To whom correspondence should be addressed. E-mail: weeks@physics.emory.edu.

\*\*The method, as it stands, is most relevant to experiments in colloidal systems probed by confocal microscopy. From a theoretical and simulational point of view it is extendable to more complex molecular systems.

© 2008 by The National Academy of Sciences of the USA

answer in this article a more fundamental question: Are the Eulerian description and lattice spin variables sufficient to describe the physical characteristics of particle systems?

Below, we demonstrate on an experimental colloidal system in which the Eulerian approach accurately captures the slow dynamics of dense particle packings.

## Method

The proposal consists in transforming the data of numerical simulations or confocal microscopy experiments, usually presented in the Lagrangian representation as time-dependent positions and velocities of distinguishable particles (14–17), into time-dependent occupation numbers of a fixed array of finite-volume cubic pixels within the finite-volume box. The cubic pixels have linear size  $a = R/q$ , where  $R$  is the radius of the particles and  $q > 1$  is a parameter. The number of pixels is  $N = V/a^d$  with  $V$  the total volume of the experimental box (we focus throughout the article on the  $d = 3$  case relevant to the experiments analyzed below). The simplest definition of the spin variable is such that  $s_i = 1$  whenever a particle (independently of which one it is) overlaps the  $i$ th pixel, and  $s_i = -1$  otherwise. With such a definition, although, the magnetization density is nonzero,  $m = N^{-1} \sum_{i=1}^N s_i \neq 0$ , at a generic volume fraction  $\phi$ . To work at zero magnetization density and make closer contact with usual spin (glass) problems, we shrink the particle size to an effective radius  $R_{\text{eff}}$  such that the covered volume is 50%.<sup>††</sup>

An efficient algorithm that maps particle positions into spin variables works as follows. First, we construct the grid of pixels and sets all spins to  $s_i = -1$  for all  $i$ . Next, we read the particle centers from the data file and set to  $+1$  the spin variables at the pixels less than  $R_{\text{eff}}$  from the center of each particle. We thus avoid having to go over all sites in the lattice and to compute distances between particle centers. We repeat this procedure at each time step.

The spin variable is naturally related to an occupation number,  $n_i \equiv (s_i + 1)/2 = 0, 1$ , and then to a density. We stress here that these densities are not coarse-grained quantities built by looking at distances larger than the particle size, but on the contrary, by looking at distances of the order and below the particle size. Within this construction the parallel with the spin-glass problem is clear: a short-ranged equal-time spin–spin correlation function corresponds to a short-ranged particle density order, etc.

Our spin-mapping is similar in spirit to standard image-analysis techniques of thresholding, whereby a gray-scale image is converted into a binary (black and white) image (see, for example, ref. 18). The key difference is that, rather than applying a thresholding operation to the raw images, we work with the particle positions obtained from the raw images. Furthermore, our spin “pixels” of size  $R/5$  do not directly correspond with the pixels in the raw images; see Fig. 1. We would like to stress that our method can be also applied to simulation data, for which there never exists a “raw image.”

## Analysis

We apply this framework to experimental data from colloidal suspensions, both in the supercooled liquid regime (14, 15) and the dense glassy phase (16). The suspensions are of colloidal polymethylmethacrylate (PMMA) with radius  $R = 1.18 \mu\text{m}$  (and a polydispersity of  $\approx 5\%$ ), suspended in a mixture of decalin and either cycloheptylbromide (for the samples with  $\phi < \phi_g \approx 0.58$ )

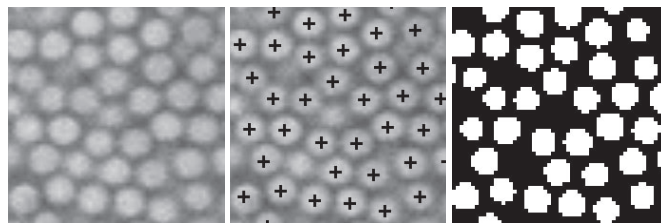


**Fig. 1.** Scheme of the data analysis. Starting from the original 3D image, we find the 3D particle positions. Particles with centers within  $R/2$  of this particular image slice are indicated. From these particle positions, spins are assigned as discussed in the text. Because the particle positions are located with subpixel accuracy and at differing  $z$  positions, the “spin images” are not circularly symmetric in a given  $z$  slice. The images correspond to the sample with  $\phi = 0.56$  and they are  $15 \mu\text{m}$  wide.

or cyclohexylbromide (for the sample with  $\phi > \phi_g$ ). These solvent mixtures match the index of refraction of the particles to aid in visualization, as well as the particle density, so that sedimentation does not occur during the experiments. In these solvents, the particles are slightly charged, modifying their pair correlation function somewhat from that of hard spheres, although they still undergo a glass transition at  $\phi_g \approx 0.58$ . The particles in dilute samples diffuse their own diameter in 11 s, although in these concentrated samples their motion is much slower (14). All samples are stirred before data acquisition. The two samples with  $\phi < \phi_g$  are stirred to break up any crystals, and data acquisition is started after transient flows have diminished ( $\approx 30$  min). For the sample with  $\phi > \phi_g$ , no crystals are present before stirring; instead, stirring initiates aging, and data acquisition begins immediately after the stirring is ended, setting the initial time  $t_w = 0$  (16).

Confocal microscopy (19) is used to rapidly obtain a three-dimensional image of dimensions approximately  $60 \times 60 \times 12 \mu\text{m}^3$ . Within each image, particle positions are obtained with an accuracy of 30 nm in  $x$  and  $y$ , and 50 nm in  $z$  (along the optical axis of the microscope). For other experimental details, see refs. 14 and 16.

We used  $q = 5$  so that  $a = R/q \approx 1.18 \mu\text{m}/5 \approx 0.236 \mu\text{m}$  that is of the order of the averaged displacement of the full sample  $r \approx 0.1 \mu\text{m}$  (14). The 3D positions of the particles were recorded every 18 s for the supercooled datasets at  $\phi = 0.52$  and  $\phi \approx 0.56$ , and 20 s for the glassy one at  $\phi = 0.62$ . The effective radii are:  $R_{\text{eff}} = 1.17 \mu\text{m}$  at  $\phi = 0.52$ ,  $R_{\text{eff}} = 1.11 \mu\text{m}$  at  $\phi \approx 0.56$  and  $R_{\text{eff}} = 1.10 \mu\text{m}$  at  $\phi = 0.62$ .

We now show how to characterize the dynamics of the colloidal system by using solely the mapped spin variables. We start by defining two-spin correlations

$$C_2(r; t, t_w) = \frac{1}{N} \sum_{i,j; |\vec{r}_i - \vec{r}_j| = r} s_i(t) s_j(t_w), \quad [1]$$

which can be used to determine both equal-time spatial correlations and same-site two-time correlations.

In Fig. 2 we present the equal-time correlation function between two spins at a distance  $r$ ,  $c(r, t) \equiv C_2(r; t, t)$ , which is analogous to the pair correlation function convolved with a square hat function of width  $R_{\text{eff}}$ . The finite sample size implies time-dependent fluctuations. In the supercooled liquid regime these are present but no systematic trend is visible (data not shown). The time dependence in the glass is shown in Fig. 2A where the pair correlation function as a function of  $r$  is displayed. The curves show no systematic time dependence until  $t \sim 4,000$  s. A clear departure is seen at later times when the pair correlation no longer decays to zero. Although we do not know the exact reason for the saturation at long distances, we can exclude

<sup>††</sup>Alternatively, one may work with fixed magnetization and subtract this constant level from the spin variables. We choose to work with the symmetric representation via the effective radius  $R_{\text{eff}}$  to remain as close as possible to a spin glass problem with zero magnetization, and thus make the analogies and comparisons between the particle and spin systems easier and clearer. Moreover, the spin clusters associated with each particle are thus disconnected, simplifying the eventual identification of an equivalent spin dynamics.

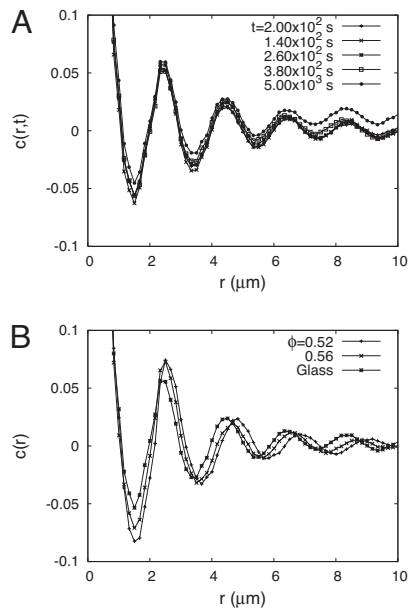


**Fig. 2.** One-time two-spin correlation  $c(r, t)$  as a function of distance  $r$ . (A) Evolution with time of the glass ( $\phi \approx 0.62$ ) pair-correlation function. All curves are very similar, apart from the last one that does not decay at long distances. See the text for a discussion on this fact. (B) The time-averaged quantity  $c(r)$  for the three packing fractions:  $\phi \approx 0.52, 0.56$ , and  $0.62$ .

crystallization because Cianci *et al.* (16) found no increase in crystalline order as the sample aged. In what follows we just analyze glass data for times that are shorter than  $t \sim 4,000$  s.

The time averages of the equal-time correlation function,  $c(r) \equiv k_m^{-1} \sum_{k=1}^{k_m} c(r, t_k)$ , are shown in Fig. 2B for the three packing fractions. These are calculated by using  $k_m = 10$  times equally spaced over an interval of approximately 6,300 s in the supercooled liquid and 8 times before 4,000 s in the glass. Notice that the peaks move slightly to lower values of  $r$  for increasing values of  $\phi$ , but there is no qualitative difference in this one-time quantity for the three packing ratios. The peak structure is essentially the same as the one shown in ref. 15 for the supercooled liquid and in ref. 16 for the glass, computed by using the particle positions, although the peaks are slightly wider and the splitting of the second peak is not resolved because of the finite-particle radius.

We now turn to two-time quantities, starting from the global equal-space two-spin correlation  $C(t, t_w) \equiv C_2(r=0; t, t_w)$ . In Fig. 3 we present its decay, as a function of  $t - t_w$ , for the supercooled liquid regime. The group of curves that fall below are for  $\phi \approx 0.52$ . The curves drawn with thin lines represent data for several waiting-times and, within the numerical error, they have the same decay, proving that the dynamics are stationary. The thick (red) line is the average over all waiting times. The thick (blue) curve lying above is the averaged data for  $\phi \approx 0.56$ . The spreading for different waiting-times (data not shown) is similar to the one for  $\phi \approx 0.52$ . In both cases,  $C$  decays from 1 to 0.8 in  $<18$  s (the minimum time step for which data are recorded), because of Brownian motion of the particles within their cages (15). The dotted black lines are exponential fits,  $e^{-(t-t_w)/\tau_e}$ , to the decay for  $t - t_w > 90$  s that have been translated to make the curve visible. The solid black line is a fit of the data for  $\phi \approx 0.56$  to a stretched exponential,  $e^{-[(t-t_w)/\tau_s]^\beta}$ . In the caption we give the values of the characteristic times,  $\tau_e$  and  $\tau_s$ , and the stretching exponent,  $\beta$ , for both densities, although in Fig. 3 we show only the stretched exponential for the higher packing fraction. In this way we recover the ubiquitous stretched exponential relaxation

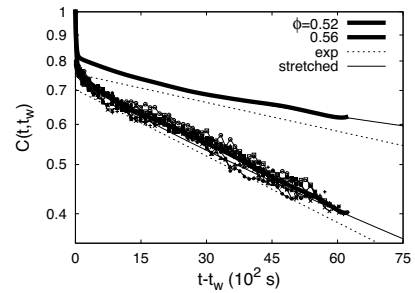


**Fig. 3.** Two-time correlation  $C(t, t_w)$  as a function of time delay  $t - t_w$  in the supercooled liquids with  $\phi \approx 0.52$  and  $0.56$ . The decay at several waiting times ( $t_w = 180, 30, 65, 414, 558, 756, 1,008, 1,350, 1,800$  s) is shown with data points connected with thin lines; the average of these sets is shown with thick lines, along with exponential (dotted line) and stretched exponential (thin solid line) fits to the averaged data. The characteristic times of the exponential and stretched exponential are  $\tau_e = 9,950$  s ( $\phi = 0.52$ ),  $23,000$  s ( $\phi = 0.56$ ), and  $\tau_s = 10,650$  s ( $\phi = 0.52$ ), and  $43,400$  s ( $\phi = 0.56$ ), respectively, and the stretching exponent is  $\beta = 0.85$  ( $\phi = 0.52$ ) and  $\beta = 0.65$  ( $\phi = 0.56$ ).

in supercooled liquids that has been observed with a large variety of techniques (20).

Fig. 4 shows the two-time correlation function in the aging regime. Fig. 4A displays the relaxation after several waiting times. As in the supercooled liquid regime, the correlation decays from 1 to 0.7 rapidly (inner cage motion) and then further decays to zero in a much slower manner (structural relaxation). In a double-logarithmic scale the separation between the stationary ( $C \geq 0.7$ ) and aging ( $C \leq 0.7$ ) regimes is seen as a plateau at the Edwards–Anderson value  $q_{ea} \approx 0.7$ . Fig. 4B demonstrates that the aging data can be satisfactorily scaled by using the “simple” aging (1) form  $C(t, t_w) \sim f(t/t_w)$  with  $f(x) \sim x^{-0.35}$  for waiting times that are longer than  $t_w \sim 1,200$  s. However, the range of variation of both axes is smaller than a decade and it is hard to give a concrete conclusion on simple aging in this sense.

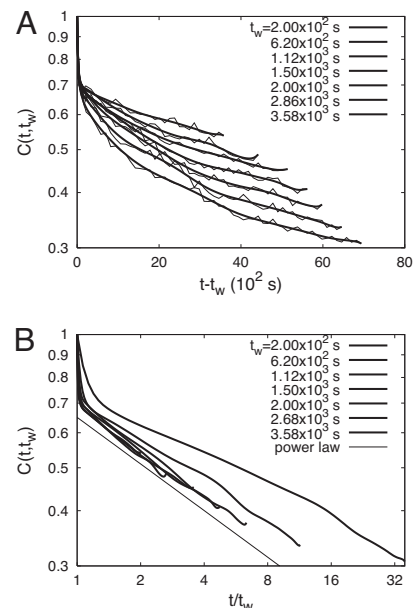


**Fig. 4.** Two-time correlation  $C(t, t_w)$  in the glass. (A) data for the decay at several waiting times ( $t_w = 200, 620, 1,120, 1,500, 2,000, 2,860, 3,580$  s) are shown with thin lines, plotted as function of the time delay  $t - t_w$ ; the smoothed decay is highlighted with thick lines. (B) Scaled data by using the simple aging form  $C(t, t_w) \sim f(t/t_w)$ ; the solid (black) line is the power law  $f(x) \sim x^{-0.35}$ .

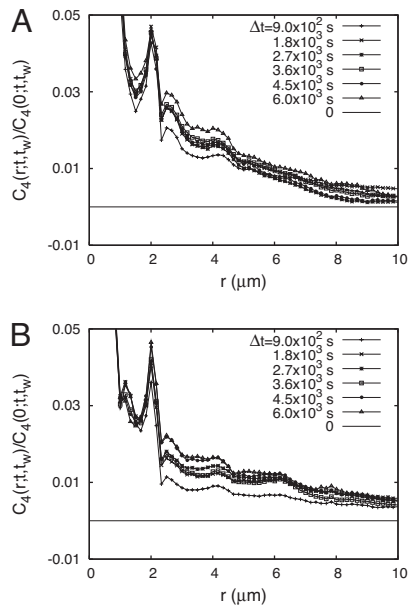


**Fig. 5.** The four-point correlation  $C_4$  in the supercooled liquid for several time delays given in the key. (A)  $\phi = 0.52$ . (B)  $\phi = 0.56$ .

Still, it is interesting to note that this behavior is remarkably similar to the one found with Monte Carlo simulations of the 3d Edwards–Anderson (EA) spin glass (21).

A two-time dependent correlation length (22, 23) can be extracted from the spatial decay of a two-sites and two-times correlation:

$$S_4(r; t, t_w) = \frac{1}{N} \sum_{i,j; |\bar{r}_i - \bar{r}_j| = r} s_i(t)s_i(t_w)s_j(t)s_j(t_w), \quad [2]$$

or a variation in which we extract the square of the two-time local correlation  $C(t, t_w)$  that is the expected large distance limit of Eq. 2:

$$C_4(r; t, t_w) \equiv S_4(r; t, t_w) - [C(t, t_w)]^2. \quad [3]$$

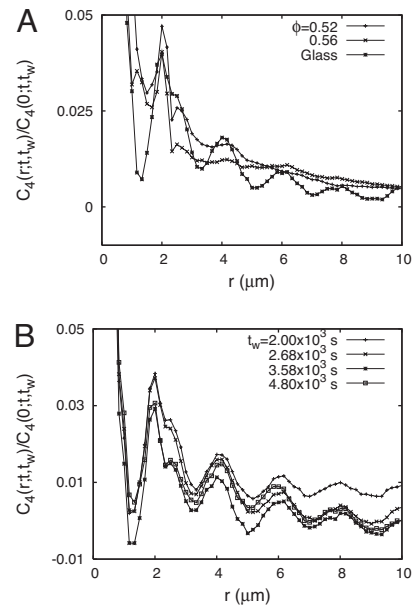
These definitions are a simple extension of the ones used in the analysis of the stationary supercooled liquid (24–28).

Fig. 5 displays the four-point correlation function  $C_4$  for several time delays in the supercooled liquid. In Fig. 6 we show its space dependence for a fixed time delay,  $t - t_w = 1,800$  s in the supercooled liquid and  $t - t_w = 2,000$  s in the glass. The supercooled liquid curves have been averaged over the waiting time taking advantage of stationarity. The glassy curve has been smoothed by averaging over two time windows of length  $\tau = 200$  s centered at  $t_w$  and  $t$ .

The correlation length can be evaluated by using

$$\xi^2 \equiv \frac{\int_0^{r_{\max}} dr r^2 C_4(r; t, t_w)}{\int_0^{r_{\max}} dr C_4(r; t, t_w)} \quad [4]$$

in the limit  $r_{\max} \rightarrow \infty$ . This analysis, applied to the data in Fig. 6, yields a correlation length  $\xi$  of the order of  $4-6R$ . This can be confirmed by simple visual inspection because all curves decay close to zero at distances  $r \approx 8-10\mu\text{m} \approx 4-6R$ . These values are of the same order as the ones found in previous studies (15).



**Fig. 6.** The four-point correlation  $C_4$  in the supercooled liquid and the glass. (A) Comparison between three packing fractions,  $\phi = 0.52, 0.56$  at  $t - t_w = 1,800$  s and the glass  $\phi = 0.62$  at  $t - t_w = 2,000$  s and  $t_w = 2,000$  s. (B)  $C_4$  for the glass at several waiting times and  $t - t_w = 1,200$  s fixed.

To capture the time dependence of  $\xi$  we use, instead,  $r_{\max} = 30a \approx 7.1 \mu\text{m}$ . The reason is that we do not have enough precision at  $r > r_{\max}$  to disentangle the curves measured at different times. We thus obtain shorter lengths,  $\xi \sim 1-1.4R$  (notice that  $\xi \leq r_{\max}$  follows from Eq. 4 for  $C_4 > 0$ ), that have, though, a systematic temporal dependence. Fig. 7 shows these results. The supercooled liquid curves follow the expected trend: the sample with a higher packing fraction ( $\phi = 0.56$  with thick green line) has a longer correlation length than the one with the lower packing fraction ( $\phi = 0.52$  with thick red line). In both cases the length smoothly increases in time. We then compare these results to the measurements in the glass at different waiting times (thin lines in the same figure). All curves grow as a function of time difference. At short time differences the curves with shorter waiting times have a longer correlation length, whereas the trend reverses at longer time differences. In the glass the growth with time difference is faster than in the supercooled liquid and one expects the longer waiting-time curves to go beyond the supercooled liquid ones at longer time differences (not reached in the experiment). The reason why the correlation lengths in the glass are shorter than the ones in the supercooled liquid at the available times is that the glass is still out of

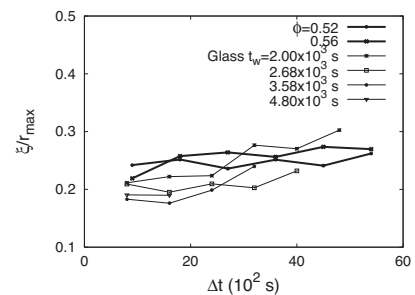


**Fig. 7.** The time dependence of the correlation length normalized by the cutoff distance  $r_{\max}$  ( $= 30$  lattice units) in the supercooled liquid and glass, computed by using Eq. 4.

equilibrium and correlations have not yet propagated far in the sample.

The two-time dependence in the glassy regime is similar to the one found in the 3d EA spin glass (21), the Lennard–Jones mixture (29, 30), and the 3d random field Ising coarsening system (31). In the latter case the origin of the two-time dependence of the growing length  $\xi$  can be traced back to the one-time dependence of the averaged radius of the growing domains of two competing equilibrium states. In the structural and spin glass cases, the two-time dependence of  $\xi$  does not have such a clear simple origin, and it is less well understood.

We now turn to the study of local correlations, which are probes of local heterogeneities in the dynamics. The particles in the colloidal system do not displace at the same rate: some regions can reconfigure much faster than others, for the same elapsed time between frames. A broad distribution characterizing these heterogeneities can be captured, in the mapped spin system, by using a local two-time spin–spin correlation averaged over a cell of size  $V_r = \ell^3$  centered at  $r$ :

$$C_\ell(\vec{r}; t, t_w) = \frac{1}{V_r} \sum_{i \in V_r} s_i(t) s_i(t_w). \quad [5]$$

Whenever the cell size  $\ell$  is much larger than the dynamical correlation length  $\xi$ , the local correlations just reflect the global value  $C(t, t_w)$ . Instead, whenever the coarse-graining box  $\ell$  is smaller than  $\xi$ , the local values are nonuniform. This fact is captured by a broad probability distribution function (PDF)  $P(C_\ell)$  at fixed times  $t$  and  $t_w$ . A simple scaling hypothesis implies (21, 23)

$$P(C_\ell; t, t_w, \ell, \phi) = P(C_\ell; C, \ell/\xi, \ell/L \rightarrow 0, \phi), \quad [6]$$

with  $C$  and  $\xi$  the values of the global correlation and correlation length at the measuring times  $t$  and  $t_w$ , and  $L$  the size of the sample that is much longer than the coarse-graining length. We kept an explicit dependence on the control parameter in the system, that is to say, the packing fraction  $\phi$ . This form is obtained by exchanging the dependence on times  $t$  and  $t_w$  by a dependence on the two-time quantities  $C$  and  $\xi$  (exploiting their monotonicity properties) and then assuming that the three lengths  $L$ ,  $\xi$ , and  $\ell$  can only appear through the ratios  $\ell/\xi$  and  $\ell/L$ . Because the time variation of the correlation length is very slow, as a first approximation one can neglect the scaling variable  $\ell/\xi$ . In Fig. 8 we test the scaling form  $P(C_\ell; C, \phi)$  (22, 32) by using a coarse-graining box  $\ell = 2.2R \approx 2.60 \mu\text{m}$ . The PDFs are shown for different values of the waiting time for the two supercooled systems at  $\phi \approx 0.52$  (Fig. 8A) and  $\phi \approx 0.56$  (Fig. 8B), and for the glass with  $\phi \approx 0.62$  (Fig. 8C). The PDFs collapse for fixed time difference  $\Delta t = t - t_w$  in the case of the supercooled samples, and for fixed ratio  $t/t_w$  in the case of the glass, reflecting that time-translation invariance is manifest in the supercooled liquid regime, but broken in the glass, which ages. (In the case of Fig. 8B, the bad collapse for  $t_w = 900$  s may be attributed to lack of equilibration at this high packing fraction: fluctuations may be more sensitive than average values in detecting a remnant time variation. Another explanation would be that the two distributions are sampling two different windows in time, one of which happens to have more activity than the other.) As expected, the PDFs get wider for longer time differences or larger values of  $t/t_w$ .

Remarkably, once the PDFs have been scaled, the scaling function of the sample with low packing fraction is very similar to the one of the glass. It is worth noting here that the average correlations in the loose supercooled liquid and the glass are very similar:  $\langle C \rangle \sim 0.5$ . The averaged two-time correlation in the dense supercooled liquid remains, during the available time window, too high to be used and compared with the other two

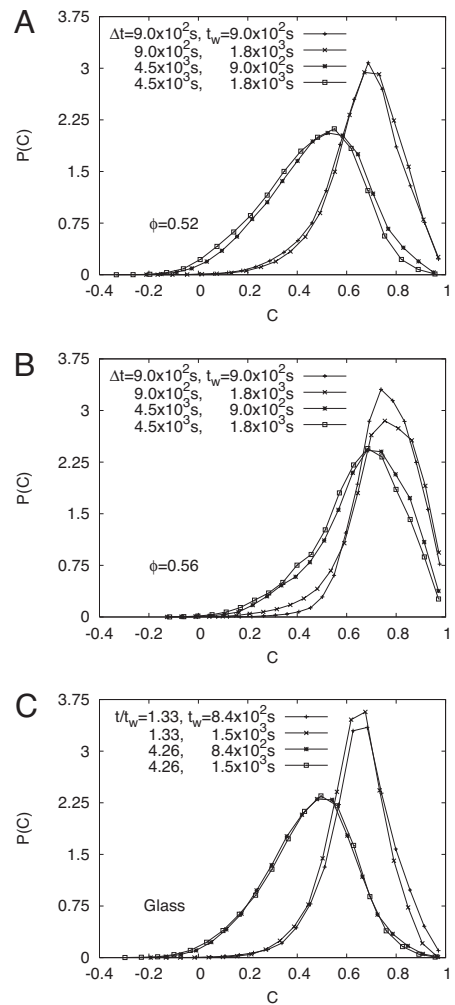


**Fig. 8.** The PDFs for local two-time spin–spin correlations for supercooled liquid at  $\phi \approx 0.52$  (A), supercooled liquid at  $\phi \approx 0.56$  (B), and the glass at  $\phi \approx 0.62$  (C). The distributions signal heterogeneous dynamics within regions of linear size  $\ell = 2.2R = 2.60 \mu\text{m}$ . Supercooled systems show data collapse at fixed time differences  $t - t_w$ , reflecting time-translation invariance, whereas the glassy sample shows data collapse at fixed  $t/t_w$ , reflecting approximate simple aging behavior.

cases. Its PDF has strong contributions from inner-cage dynamics that cannot be disentangled. The similarity between the PDFs for  $\phi \approx 0.52$  and  $0.62$  suggests that a “universal” PDF connecting the fluctuations for different packing fractions through a proper rescaling of times might exist. We plan to explore this hypothesis by using molecular dynamics of Lennard–Jones mixtures.

## Conclusions

In short, we proposed an Eulerian formulation of the particle dynamics of supercooled liquids and glasses. Such formulation does not rely on tracking individual particles over time, but instead it focuses on fixed locations at each time, without regard to the particle identity at the given site. This approach permits the study of dynamical heterogeneities within a fixed frame of reference similar to the one used for spin models (21–23, 31).

We assessed the validity of this Eulerian approach by testing it on real experimental data on colloidal particles. We devised a simple method to translate particle data position into fixed frame spin variables, and then used methods common in the analysis of the dynamics of spin glasses. We computed correlation functions and extracted a correlation length from confocal

microscopy data of supercooled and glassy samples and we found remarkably similar results to the ones obtained with numerical simulations of spin models.

This approach should motivate the construction of effective spin models aimed at representing the physics of particle systems. The fundamental spin variables in such constructions should correspond to microscopic densities at scales of the order and below the particle size, and the kinematics of these spins should be highly constrained because of the requirement that these spins encode extended objects, the original particles. This perspective provides a new, more microscopic physical motivation to the study of kinetically constrained models, in which the spins are variables at short length scales and not some large-distance (much bigger than the particle sizes) phenomenological measure of heterogeneous dynamics (12, 13). The spin-type formulation also suggests that an effective model that relates spin glasses and structural glasses should involve interactions among many of the spins, similarly to the  $p$ -spin models (1, 3–8), so as to account for the constituent relations that the spins encode extended objects of sizes bigger than the lattice spacings. It also suggests that in these models there should be frustration between short-range

ferromagnetic interactions that cluster the mapped spins making up the particles and the longer-range antiferromagnetic interactions that encode the interparticle repulsions. This is somehow reminiscent of ideas surveyed in ref. 33.

The main result of our work is that it establishes on firm grounds, by critically testing the Eulerian formulation on real physical systems of dense colloidal particles, the notion that the particle dynamics in supercooled liquids and glasses can be faithfully described in terms of spin variables and analyzed much as in spin-disordered models. It thus provides the foundation on which to justify building effective spin models so as to capture the physics of the particle systems.

**ACKNOWLEDGMENTS.** L.F.C. thanks the Universidad Nacional de Mar del Plata, Argentina, and Boston University, G.F. thanks the Abdus Salam International Centre for Theoretical Physics, Trieste, Italy, and C.C., G.F., and J.L.I. thank the Laboratoire de Physique Théorique et Hautes Energies, Jussieu, France, for hospitality during the preparation of this work. This work was supported by National Science Foundation Grants DMR-0403997 (to C.C.) and DMR-0239109 (to E.R.W.) and by Project International de Collaboration Scientifique 3172, Proyecto de Investigación Plurianual 5648, and Proyecto de Investigación Científica y Tecnológica 20075 (to L.F.C., G.F., and J.L.I.). L.F.C. is a member of Institut Universitaire de France.

- Cugliandolo LF (2003) Dynamics of glassy systems in slow relaxation and non equilibrium dynamics in condensed matter, Les Houches Session 77, eds Barrat J-L, et al. (Springer, Berlin), arXiv:cond-mat/0210312v2.
- Binder K, Kob W (2005) *Glassy Materials and Disordered Solids: An Introduction to Their Statistical Mechanics* (World Scientific, Singapore).
- Kirkpatrick TR, Thirumalai D (1987)  $p$ -spin-interaction spin-glass models: Connections with the structural glass problem. *Phys Rev B* 36:5388–5397.
- Kirkpatrick TR, Thirumalai D (1988) Comparison between dynamical theories and metastable states in regular and glassy mean-field spin models with underlying first-order-like phase transitions. *Phys Rev A* 37:4439–4448.
- Kirkpatrick TR, Thirumalai D (1988) Mean-field Potts glass model: Initial-condition effects on dynamics and properties of metastable states. *Phys Rev B* 38:4881–4892.
- Kirkpatrick TR, Wolynes P (1987) Connections between some kinetic and equilibrium theories of the glass transition. *Phys Rev A* 35:3072–3080.
- Kirkpatrick TR, Wolynes P (1987) Stable and metastable states in mean-field Potts and structural glasses. *Phys Rev B* 36:8552–8564.
- Kirkpatrick TR, Thirumalai D, Wolynes P (1989) Scaling concepts for the dynamics of viscous liquids near an ideal glassy state. *Phys Rev A* 40:1045–1054.
- Cugliandolo LF, Kurchan J (1993) Analytical solution of the off-equilibrium dynamics of a long-range spin-glass model. *Phys Rev Lett* 71:173–176.
- Tarzia M, Moore MA (2007) Glass phenomenology from the connection to spin glasses. *Phys Rev E* 75:031502.
- Grigera TS, Martin-Mayor V, Parisi G, Verrocchio P (2004) Asymptotic aging in structural glasses. *Phys Rev B* 70:014202–014205.
- Fredrickson GH, Andersen HC (1984) Kinetic Ising-model of the glass-transition. *Phys Rev Lett* 53:12441247.
- Fredrickson GH, Andersen HC (1985) Facilitated kinetic Ising-models and the glass-transition. *J Chem Phys* 83:58225831.
- Weeks ER, Crocker JC, Levitt AC, Schofield A, Weitz DA (2000) Three-dimensional direct imaging of structural relaxation near the colloidal glass transition. *Science* 287:627–631.
- Weeks ER, Crocker JC, Weitz DA (2007) Short and long range correlated motion observed in colloidal glasses and liquids. *J Phys C Condens Matter* 19:205131–205142.
- Cianci GC, Courtland RE, Weeks ER (2006) Correlations of structure and dynamics in an aging colloidal glass. *Solid State Commun* 139:599–604.
- Wang P, Song C, Makse HA (2006) Dynamic particle tracking reveals the aging temperature of a colloidal glass. *Nat Phys* 2:526–531.
- Russ JC (2002) *The Image Processing Handbook* (CRC Press, Boca Raton, FL), 4th Ed, Chap 6.
- Prasad V, Semwogerere D, Weeks ER (2007) Confocal microscopy of colloids. *J Phys Condens Matter* 19:113102.
- Phillips JC (1996) Stretched exponential relaxation in molecular and electronic glasses. *Rep Prog Phys* 59:1133–1207.
- Jaubert LDC, Chamon C, Cugliandolo LF, Picco M (2007) Growing dynamical length, scaling and heterogeneities in the 3d Edwards-Anderson model. *J Stat Mech* P05001.
- Castillo HE, Chamon C, Cugliandolo LF, Iguain JL, Kennett MP (2003) Spatially heterogeneous ages in glassy systems. *Phys Rev B* 68:134442.
- Chamon C, Cugliandolo LF (2007) Fluctuations in glassy systems. *J Stat Mech* P07022.
- Kob W, Donati C, Plimpton SJ, Poole PH, Glotzer SC (1997) Dynamical heterogeneities in a supercooled Lennard-Jones liquid. *Phys Rev Lett* 79:2827–2830.
- Donati C, et al. (1998) Stringlike cooperative motion in a supercooled liquid. *Phys Rev Lett* 80:2338–2341.
- Franz S, Parisi G (2000) On non-linear susceptibility in supercooled liquids. *J Phys C Condens Matter* 12:6335–6342.
- Donati C, Franz S, Parisi G, Glotzer SC (2002) Theory of non-linear susceptibility and correlation length in glasses and liquids. *J Non-Cryst Solids* 307:215–224.
- Biroli G, Bouchaud J-P (2004) Diverging length scale and upper critical dimension in the Mode-Coupling Theory of the glass transition. *Europhys Lett* 67:21–27.
- Parisi G (1999) An increasing correlation length in off-equilibrium glasses. *J Phys Chem B* 103:4128–4131.
- Parsaeian A, Castillo HE (2006) Growth of spatial correlations in the aging of a simple structural glass, arXiv:cond-mat/0610789.
- Aron C, Chamon C, Cugliandolo LF, Picco M (2008) Scaling and super-universality in the coarsening dynamics of the 3d random field Ising model. *J Stat Mech*, P05016.
- Castillo HE, Parsaeian A (2007) Local fluctuations in the ageing of a simple structural glass. *Nat Phys* 3:26–28.
- Tarjus G, Kivelson SA, Nussinov Z, Viot P (2005) The frustration-based approach of supercooled liquids and the glass transition: A review and critical assessment. *J Phys Condens Matter* 17:R1143–R1182.